Applied Physics Letters

Electrically driven on-chip transferrable micro-LEDs

Cite as: Appl. Phys. Lett. **121**, 241107 (2022); https://doi.org/10.1063/5.0111362
Submitted: 19 July 2022 • Accepted: 05 December 2022 • Published Online: 15 December 2022

Byung-Ju Min, Yeon-Ji Kim, Jae-Hyuck Choi, et al.

AIP Publishing

Applied Physics Letters ARTICLE scitation.org/journal/apl

Electrically driven on-chip transferrable micro-LEDs

Cite as: Appl. Phys. Lett. **121**, 241107 (2022); doi: 10.1063/5.0111362
Submitted: 19 July 2022 · Accepted: 5 December 2022 ·
Published Online: 15 December 2022

Byung-Ju Min,[1] Yeon-Ji Kim,[1] Jae-Hyuck Choi,[2] Min-Woo Kim,[1] Kyong-Tae Park,[1] Dong Jin Jang,[1] Jin Sik Choi,[1] and You-Shin No[1,a)]

AFFILIATIONS

[1]Department of Physics, Konkuk University, Seoul 05029, South Korea
[2]Space Optics Team, Advanced Instrumentation Institute, Korea Research Institute of Standards and Science, 267 Gajeong-ro, Yuseong-gu, Daejeon 34113, South Korea

[a)]Author to whom correspondence should be addressed: ysno@konkuk.ac.kr

ABSTRACT

In this study, we report the experimental demonstration of electrically driven on-chip transferrable microdisk light-emitting diodes (LEDs). A vertical *p–i–n* doped AlGaInP microdisk, including multi-quantum-well structures, is top-down-fabricated, on-chip micro-transferred, and converted into single micro-LEDs. Optically transparent and mechanically flexible multilayered graphene sheets are judiciously designed and introduced to the top and bottom surfaces of a single microdisk, thereby forming the top and bottom contacts. Using electroluminescence measurements, the fabricated micro-LEDs are characterized; they exhibit diode-like transport behaviors, spectroscopic light-out vs current (*L–I*) characteristics, and polarization-resolved emission properties. We believe that the proposed all-graphene-contact approach offers a direct and easy current injection scheme and further helps electrify various on-chip transferrable microarchitectures.

The on-chip integration of nano- and/or micro-scale materials and structures has become one of the critical processes to realize many photonic applications.[1–31] In particular, as most photonic platform materials suffer from the primary challenge of generating light, the efficient coupling of high-quality light sources with a photonic integrated circuit (PIC) has garnered interest among many researchers.[3–31] For example, various types of III–V semiconductor micro- and nanolasers,[12–30] such as microrings,[15,16] microdisks,[17–21] nanowires (NWs),[21–27] micropillars,[28] and photonic crystals,[29,30] are heterogeneous- and hybrid-integrated to silicon,[9–11,15,18] III–V semiconductor,[21,28] metal,[23,24] lithium niobate (LN),[31] polymer,[6] and/or silicon nitride[22,26] waveguides via low-temperature surface modification,[11,15,28] die-to-wafer bonding,[11,18] planarization,[4,8,17,18] and the membrane transfer-printing method.[16,32] In addition, the increasing demand for miniaturization necessitates not only the use of ultrasmall light sources but also their precise on-demand integration with other passive building blocks in a PIC. For example, individual III–V semiconductor light sources, modulators, and detectors have been separately integrated with silicon, LN, or low-loss polymer waveguides.[5,6,10,11] Furthermore, recent advances in the transfer-printing technique have enabled the delicate align-integration of key optical elements into highly dense and compact PICs.[7]

Another focus of interest in PIC research has been the development of a stable scheme for operating integrated light sources with electrical pumping.[3,4,15,17–19,22–26,28,30] In addition to all the advances in the technologies to control light signals in passive elements with electrical inputs,[9] it is often regarded as a key step for completing the PIC for practical applications. However, despite the demonstrations of electrically pumped light generation using III–V/II–VI semiconductors and various low-dimensional nanomaterials,[17–19,22–26] electrifying on-chip integrated light sources remains a prime challenge because of several levels of technological difficulties: (i) the precisely aligned micro-transfer of individual light sources,[15,16,18,28,30] (ii) the introduction of contacts to electrically doped and three-dimensionally unleveled nano- and microstructures or materials without electrical shortages,[15,17,22–24,28] and (iii) stable light generation and its coupling with other passive components without causing significant optical losses.[15,17,18,22–24]

In this regard, recent efforts on using structured polymers in micro-transfer for precise integration[14,20,21,26,27] and flexible and transparent graphene contacts for the electrification of single devices[19,25,26] have demonstrated the possibility to address the major challenges and difficulties. In addition, a combined approach involving the use of both technologies has been recently explored, confirming its methodological feasibility,[26] although there have been some concerns related to

the operational condition and performance of devices. In this work, we explore the abilities of the aligned micro-transfer and all-graphene-contact approach and realize an electrically driven on-chip transferrable all-graphene-contact micro-light-emitting-diode (micro-LED). We top-down-fabricate vertical *p*–*i*–*n* doped AlGaInP microdisks with multi-quantum-wells (MQWs), align-micro-transfer on a device chip using structured polydimethylsiloxane (PDMS), and fabricate them into micro-LEDs by introducing lithographically patterned graphene contacts. We perform electroluminescence (EL) spectroscopy to characterize the electrical and optical properties and demonstrate the robustness of the proposed all-graphene-contact approach. We also compare the micro-LED devices with our previous work and discuss several improvements in terms of their electrical and optical properties.

Figure 1(a) shows a schematic of the proposed on-chip transferrable all-graphene-contact electrically driven micro-LED device. A vertically doped single semiconductor microdisk, including an optical gain medium, is on-demand micro-transferred to a substrate, where the outer metallic electrodes are pre-defined. Optically transparent and mechanically flexible graphene sheets[33,34] are introduced at the top and bottom surfaces of the microdisk, thereby forming the patterned top and bottom contacts. These contacts allow for the stable injection of carriers within the patterned area into the microdisk and enable the robust radiative recombination and subsequent strong light emission. Figure 1(b) shows the false-colored scanning electron microscope (SEM) image of a fully fabricated micro-LED device. A vertical *p*–*i*–*n* doped AlGaInP microdisk, including MQWs, is located in the middle of the Cr/Au electrodes on the SiO_2 substrate. The microdisk is

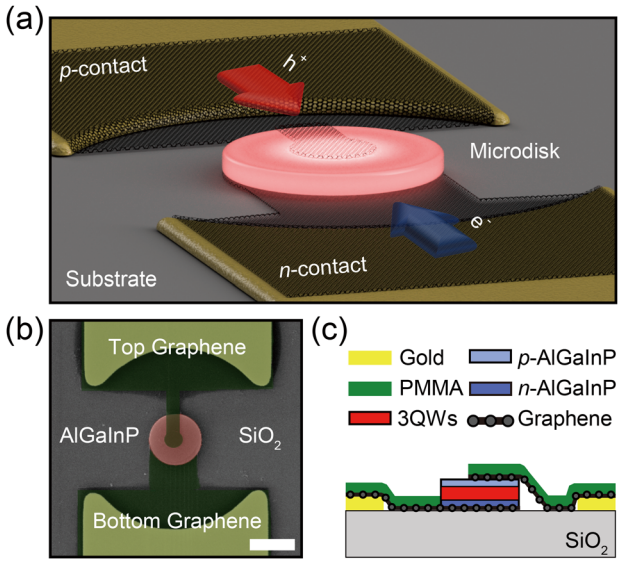

FIG. 1. (a) Schematic showing an electrically driven on-chip transferrable all-graphene-contact micro-LED device. Carriers (blue and red arrows) are injected into the active semiconductor microdisk via patterned graphene contacts that are kept in contact with the top and bottom surfaces of the microdisk. (b) False-colored SEM image of the fabricated micro-LED device. Scale bar: 5 μm. (c) Schematic illustrating the cross section of the device in (b). *p*-type top (light navy) and *n*-type bottom (dark navy) surfaces of the AlGaInP 3QW (red) microdisk are electrically connected to Au electrodes via PMMA (green)-patterned top and bottom graphene contacts (black dots and lines).

then electrically connected to the outer electrodes via the poly-methyl methacrylate (PMMA)-patterned top (*p*-type) and bottom (*n*-type) graphene contacts. Consequently, electrons and holes can be readily injected into the microdisk and radiatively recombined in the MQWs, which enables a bright light emission. Figure 1(c) presents the cross-sectional schematic of the electrically driven on-chip transferrable all-graphene-contact micro-LED.

For device fabrication, we used an epitaxially grown, vertical *p*–*i*–*n* doped, 200-nm-thick AlGaInP/GaInP MQW slab-type wafer [Fig. 2(a) and Fig. S1]. The AlGaInP spacer between the highly doped *p*- or *n*-contact and the intrinsic layers serves as an intermediate conducting layer to help smooth injection of current. In addition, a slightly lower index of the spacer, which sandwiches the higher index MQWs, serves as an optical cladding and enables for the index-guiding of optical fields. Microdisks with various diameters ranging from 5 to 6 μm were top-down-fabricated using conventional semiconductor microfabrication techniques, including electron-beam lithography (EBL), chemically assisted ion beam etching (CAIBE), and oxygen plasma treatment [(i), Fig. 2(b)]. In particular, a 500-nm-thick AlAs layer was selectively wet-etched in a digitized manner using the buffered oxide etchant (BOE, J.T. Baker, 40% NH_4F:49% HF = 10:1). Subsequently, the microdisks with small diameters were first separated and weakly placed in the vicinity of their original positions on the growth substrate [(ii), Fig. 2(b)]. Next, we used the previously developed PDMS-microtip-assisted transfer technique to pickup the single microdisk [Fig. 2(c)]. A oxygen plasma-treated micro-cubical PDMS with a size of $20 \times 20 \times 20\ \mu m^3$ was firmly attached to a slide glass mounted on a movable XYZ stage with nanoscale translational steps. Under an optical microscope system, the microtip was align-approached to a single microdisk to establish contact [(i), Fig. 2(c)] and separate it from the growth substrate [(ii), Fig. 2(c)]. An optical microscope image exhibits the selected single microdisk after the separation [(iii), Fig. 2(c)]. The slide glass with the microtip and sample was then taken to a vicinity of the target site in a SiO_2 device substrate [(i), Fig. 2(d)] and again precisely align-approached to register the microdisk at the on-demand site [(ii), Fig. 2(d)]. Here, before the micro-transfer, we separately metalized the device substrate, wet-transferred a sheet of multilayered graphene (MLG), and conformally covered the entire substrate. The captured image shows the process of target-registering the microdisk [(iii), Fig. 2(d)]. The SEM image exhibits the align-transferred microdisk on top of the MLG sheet [(i), Fig. 2(e)]. For the definition of the graphene contact, we used high-dosage electron-beam currents and formed cross-linked PMMA patterns. These patterns protect a selective area of the graphene during oxygen plasma etching and define the final configuration of the top and bottom graphene contacts [(ii) and (iii), Fig. 2(e)]. In this device, we designed a small disk-shaped top pattern with a diameter of $\sim 2\ \mu$m at the center of microdisks to define a local region where the carrier recombination primarily occurs. We also expected that the PMMA-air index contrast might help improve light extraction in the out-of-plane direction. Three-dimensional (3D) numerical simulation results indicate a range of the top pattern diameter that sustains a strong vertical light extraction, thereby supporting our design of the top pattern [Fig. 2(f)]. We note that this vertical graphene contact approach directly addresses the issues in the conventional method, which stem from the lithographical difficulties in defining the top and bottom contacts on microstructures in a vertical fashion without electrical shortages. In addition, evaporation-based

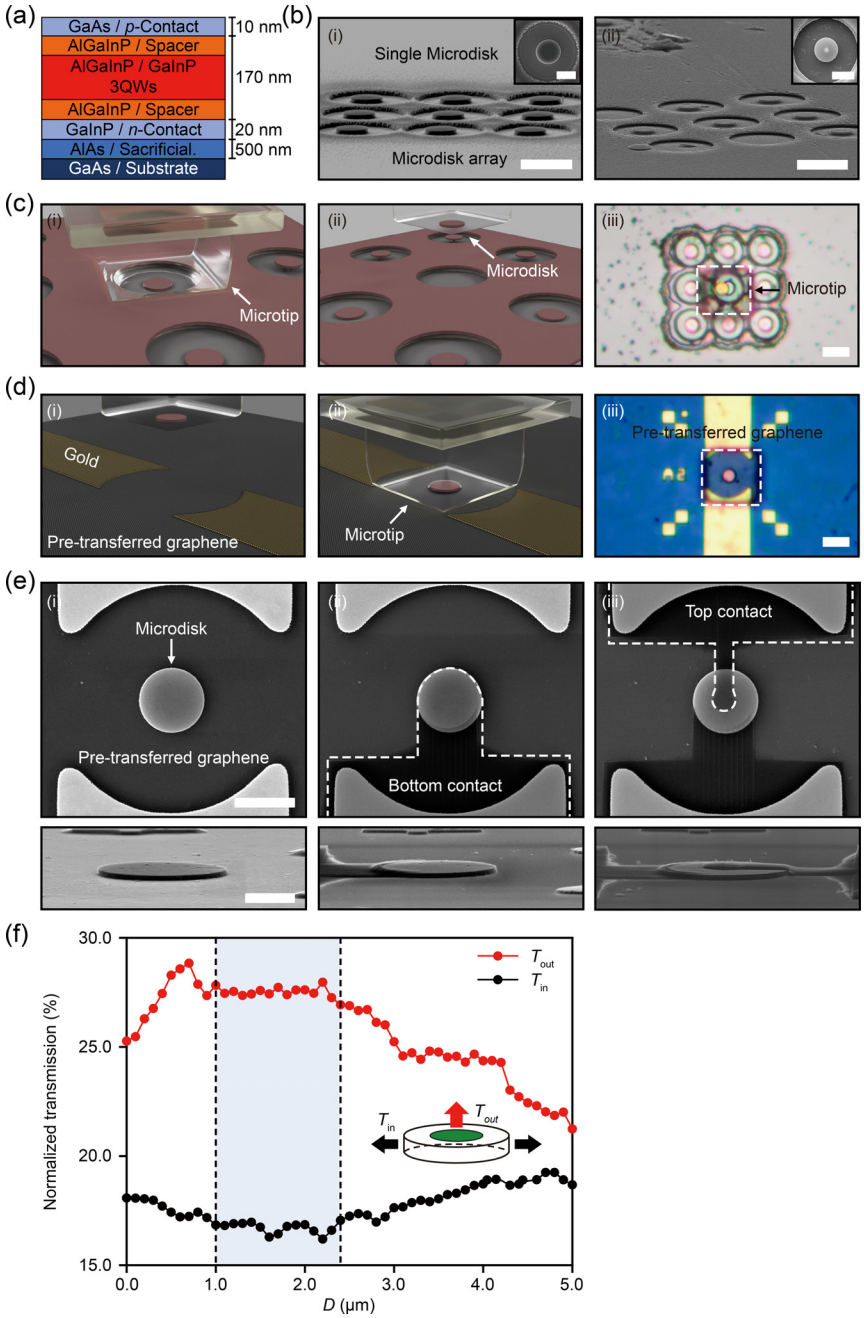

FIG. 2. (a) Detailed material and compositional design of the AlGaInP/GaAs LED wafer. (b) Tilt-view SEM images showing a 3×3 array of top-down-fabricated microdisks before (i) and after (ii) the selective chemical etching. Scale bar: 10 μm. Inset: magnified top-view SEM images of a single microdisk with a diameter of $\sim$5.5 μm. Scale bar: 4 μm. (c) PDMS microtip-assisted single microdisk pickup and separation process: (i) align-approach to and contact with a target microdisk in the growth substrate, (ii) pickup and separation of the sample from the substrate, and (iii) optical image showing the selected single microdisk that was attached to the bottom surface of the PDMS microtip. Scale bar: 10 μm. (d) Align-registration process: (i) taken to a target site in the device chip and (ii) align-registration and detach of the microdisk from the PDMS microtip. White dotted lines: PDMS microtip. Scale bar: 10 μm. (e) All-graphene-contact device fabrication: (i) Top-view SEM image (top) showing the align-transferred microdisk on bottom graphene. Lithographic definition of bottom (ii) and top (iii) graphene contacts by using the cross-linked PMMA patterns. Scale bar: 5 μm. The tilt-view SEM images of the following fabrication are at the bottom. Scale bar: 2 μm. (f) Calculated transmissions toward the in-plane (T_{in}, black dots) and out-of-plane (T_{out}, red dots) directions as a function of the size (D) of the top PMMA/graphene pattern (green disk, inset). Blue-shaded area indicated the range of D that sustained high T_{out} and low T_{in}. A magnetic dipole source with a wavelength of 700 nm was introduced at the center of the microdisk. Normalized transmissions were calculated by dividing the upward and lateral output powers by the total output power.

metal deposition often entails unexpected cracks and disconnections[17,24] when applied to topographically unleveled surfaces with high verticality. Therefore, it inevitably results in an increase in the device resistance and thermal heating, which occasionally requires additional planarization and lithography processes.[4,17,18] However, as the graphene contact is highly flexible, it conforms to the vertically structured surfaces well; it can, thus, establish a robust current path without the aforementioned issues. Furthermore, a locally loaded vertical pressure on the flexible graphene during the PDMS micro-transfer process followed by a rapid thermal annealing (RTA) process can synergistically serve to smoothen the rough surface over a large area of the graphene [Fig. S2(a)–S2(c)]. This surface modification can beneficially increase the quality of contact at the interface.

To investigate the electrical and optical properties of the fabricated device, we performed EL spectroscopy [Fig. 3(a)]. The fully fabricated device chip shown in Fig. 2(e) was tightly mounted on an XYZ stage with nanoscale translation steps. A semiconductor analyzer (Keithley 4200-SCS) generated the pulsed currents with a repetition

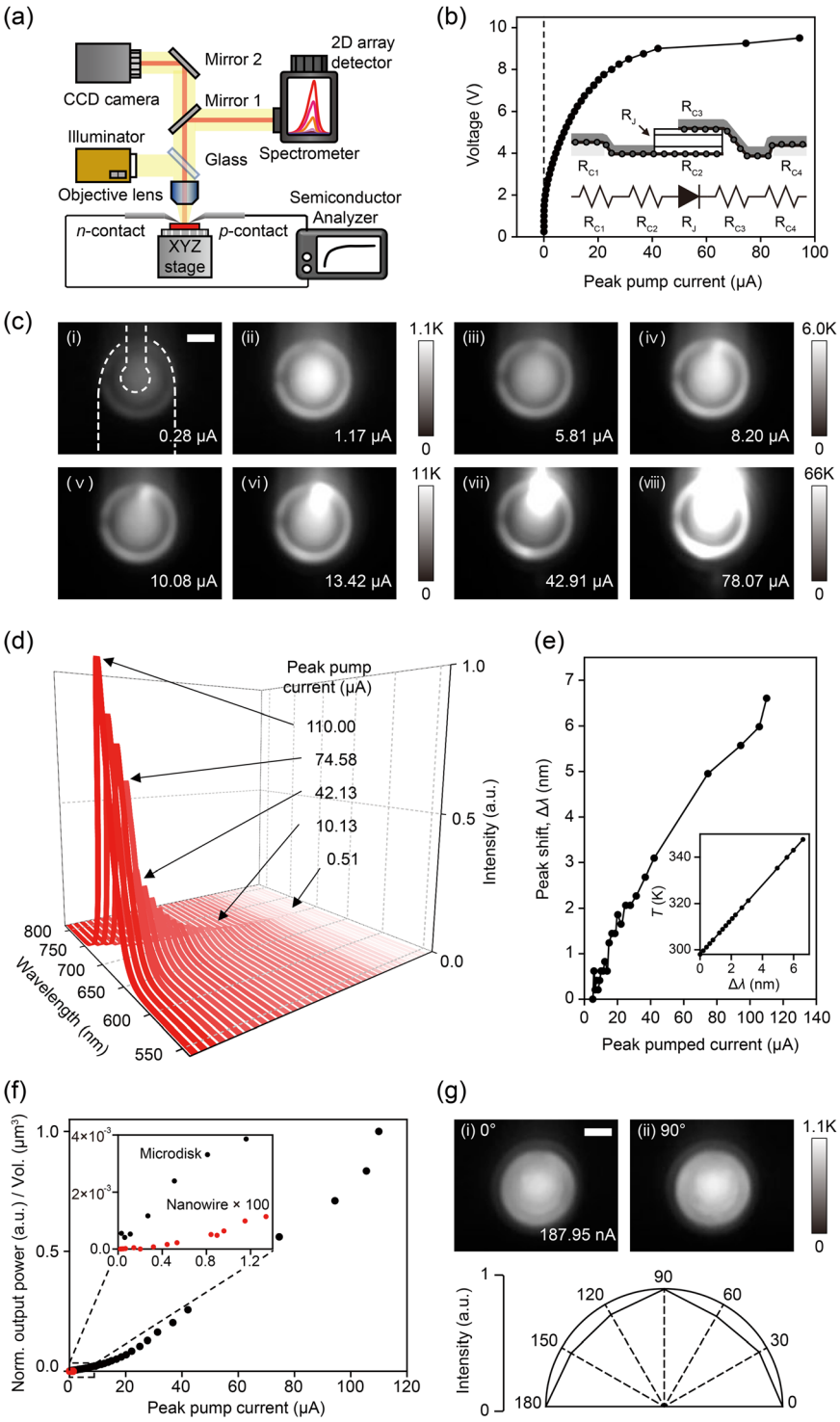

FIG. 3. (a) Schematic of the EL spectroscopy setup. (b) Measured *I–V* curve of the micro-LED device, exhibiting diode-like characteristic transport properties. Inset: the total resistance consisting of a series of contact resistances, including PMMA/MLG/Au (R_{C1} and R_{C4}), *n*-AlGaInP/MLG/SiO_2 (R_{C2}), and PMMA/MLG/*p*-AlGaInP (R_{C3}) and junction resistance (R_J). (c) EL emission profiles captured by CCD: $I_{pump} = 0.28$ (i), 1.17 (ii), 5.81 (iii), 8.20 (iv), 10.08 (v), 13.42 (vi), 42.91 (vii), and 78.06 μA (viii). For two adjacent images, the intensities were normalized with the maximum values (I_{max}): for example, for (i) and (ii), $I_{max} = 1.1 \times 10^3$; for (iii) and (iv), $I_{max} = 6.0 \times 10^3$; for (v) and (vi), $I_{max} = 11.0 \times 10^3$; for (vii) and (viii), $I_{max} = 66.0 \times 10^3$. White dotted lines indicate the top and bottom graphene contacts. Scale bar: 2 μm. (d) Measured EL spectra with different values of I_{pump}. All spectra were normalized with the maximum peak intensity. (e) A plot of peak shift ($\Delta\lambda$) as a function of I_{pump}. Inset: the estimated junction temperature (T) as a function of $\Delta\lambda$. (f) Characteristic *L-I* curve. Inset: for low $I_{pump} < 1.5$ μA, the *L–I* curve from the NW LED device in Ref. 26 was co-plotted for a direct comparison. For both plots, the output intensities were divided by the volume of optical gain in the respective devices and normalized with the maximum value. Intensities of the NW LED were increased hundred-fold for clarity. (g) CCD images of vertically (0°, top left) and horizontally (90°, top right) polarized EL emissions. Scale bar: 2 μm. Semi-polar plot of angular distribution of EL. $I_{pump} \sim 188$ nA for all angle-resolved measurements.

rate of 20 Hz and a duty cycle of 10%. These currents were injected into the micro-LED device through tungsten probe-tips that were kept in contact with the outer Cr/Au electrodes. The EL from the device was then collected by a ×50 microscope objective lens with a numerical aperture of 0.42 (Mitutoyo, M Plan APo) and fed into a spectrometer or imaged onto a charge-coupled device (CCD). We first recorded the current–voltage (*I–V*) response to investigate the electrical transport properties [Fig. 3(b)]. The results indicate a gradual

increase in the current under a low forward bias voltage of < 6 V and the onset of a nonlinear increase in the current flow at ~8.5 V. For reverse bias voltages, no measurable currents were observed. The total resistance is ~10 kΩ. This diode-like characteristic directly indicates that the injected carriers pass through the vertical *p*–*i*–*n* junctions of the device. Consequently, it confirms that the top and bottom graphene contacts robustly serve as electrical contacts. For a detailed and extended analysis on transport properties, we devised a series of control experiments (Fig. S3). First, we measured the individual contact resistances of PMMA/MLG/Au electrodes, PMMA/MLG/*p*-AlGaInP, and *n*-AlGaInP/MLG/SiO_2. Second, we repeated these experiments under several different temperature conditions ranging from 298 to 380 K and investigated their temperature-dependent properties. As anticipated, the result showed that a major contribution to the overall resistance of a micro-LED device originated from the contact resistance between the graphene and semiconductor. For example, the contact resistances of MLG/*p*-AlGaInP and *n*-AlGaInP/MLG were measured as ~5.6 and ~4.1 kΩ at room temperature, whereas that of MLG/Au was measured as ~0.042 kΩ. Based on these results, we were able to estimate the overall series contact resistance of a typical micro-LED device as ~9.8 kΩ. If we apply this value to the device in Fig. 3(b), we can readily derive the differential junction resistance as ~0.2 kΩ at room temperature. Although there exists differences in individual devices due to fabrication imperfections and material qualities, one can conservatively apply this value to the devices with similar physical dimensions. In addition, we observed that these contact resistances were improved as the temperature increased, which led to the reduced overall resistance in a micro-LED device. Detailed *I*–*V* characteristics as a function of temperature are presented in Fig. S4.

For optical characterization, we gradually increased the pump currents (I_{pump}) and observed the EL emission patterns from the device [Fig. 3(c) and Fig. S5]. At a low I_{pump} of ~0.28 μA, the emitted EL intensities started being developed into a uniform circular pattern on the central area of the microdisk at which the top graphene contact was lithographically defined [(i), Fig. 3(c)]. This EL pattern experimentally confirms that the carrier recombination primarily occurs through the disk-shaped top-graphene pattern [Fig. S6(b)]. As I_{pump} increased, the EL emissions were gradually intensified but the circular profile was kept unchanged until I_{pump} reached at 8.2 μA [(ii)–(iv), Fig. 3(c)]. However, for $I_{pump} > 10.08$ μA, a small and localized light spot along with the central EL emission started growing in intensity near the upper boundary of the microdisk at which the top graphene contact was overlapped [(v), Fig. 3(c)]. Unexpectedly, as we further increased I_{pump}, the emissions from the localized light spot were further intensified and became a major part of the entire EL emissions [(vi)–(viii), Fig. 3(c)]. We believe that these observations can be partly attributed to the formation of sidewall contact between the top-graphene and the upper side of microdisk [Fig. S5(a)], which enabled to facilitate a substantial number of carriers to be non-uniformly transported through the *p*–*i*–*n* junctions near the boundary and radiatively recombined.

We further characterized the spectroscopic properties of the proposed on-chip transferrable micro-LED device by systematically increasing I_{pump} and measuring the EL spectra [Fig. 3(d)]. The measured spectra showed a peak wavelength of ~700 nm, which represents the central emission wavelength of AlGaInP/GaInP MQWs and exhibited a gradual increase in the peak intensity with I_{pump}. In addition, we observed a gradually increasing peak shift ($\Delta\lambda$) as the I_{pump} increased [Fig. 3(e)]. This can be explained by self-heating of MQWs active medium due to the high levels of current injection and the subsequent modification of the electronic band structure of the medium. Based on these data, we also estimated the junction temperatures arising from the self-heating effect by using the temperature coefficient of the wavelength shift of the AlGaInP LED wafer ($dT/d\lambda = 7.5$ K/nm) [inset, Fig. 3(e)].[35]

Next, we summarized the intensity results of Fig. 3(d) in the conventional light-out vs current (*L*–*I*) curve, which clearly indicated a linear dependence of the output power on the I_{pump} [Fig. 3(f)]. Here, we co-plotted the *L*–*I* curve from our previous work involving NW LEDs[26] and compared both devices to examine the light emitting performance (red dots in the main panel and inset). For a quantitative comparison, we divided the output power by the volume of the gain material of respective devices (i.e., $P_{out,\ MD}/V_{MD}$, $P_{out,\ NW}/V_{NW}$) and normalized them with the maximum value. Important improvements were noted. First, we could stably operate the fabricated micro-LEDs over a broad range of I_{pump}, from a few tens of nA to > 100 μA, under low bias voltages of < 10 V. In the previous work, the typical operating voltage of NW LEDs was limited in the range 12–15 V, and the corresponding currents were less than 1 μA. Thus, the micro-LED devices exhibit a substantially reduced resistance (~10 kΩ) as compared with the NW LEDs. We also note that these improved electrical properties (i.e., the operating voltage, current level, total device resistance, etc.) are comparable to and/or even better, to some extent, than other graphene-contact-based electrically pumped light sources with similar dimensions. For example, the microdisk lasers fabricated on the epitaxial growth wafer using a top graphene contact exhibited the total device resistance of 5.8 kΩ similar to that of our micro-LED devices.[19] Single nano-LED devices, which used synthesized InGaN/GaN core-shell NWs and exhibited the comparable processes of device fabrication, including a graphene *p*-contact, were mainly operated under the similar voltage range < 10 V but a few times lower levels of currents than those of our devices.[25] Importantly, considering the double semiconductor-graphene interfaces, in contrast to the above examples, our micro-LED devices exhibit an excellent electrical performance. Furthermore, regarding light emission, we achieved a drastic increase in the output power from the micro-LED devices: an approximately 10^4-fold increase in the maximum output power was achieved. These improvements can be partly explained by the increased size of the micro-LED devices, which correspondingly enlarged the contact area and possibly resulted in a reduced resistance and an increased current flow. We believe that these electrical and optical improvements enable the micro-LEDs to readily produce strong light signals, satisfying the requirements for light sources in large circuits. Finally, we briefly investigated the polarization property of the fabricated micro-LED devices by performing angle-resolved spectroscopy [Fig. 3(g)]. A linear polarizer was used in front of either the CCD or spectrometer. As anticipated, the EL emissions recorded by the CCD and the semi-polar plot of the measured intensities showed no noticeable preferences in polarization. This result is primarily attributed to the high geometrical symmetry of the device and the unpolarized nature of spontaneous emission.

In conclusion, we demonstrated an on-chip transferrable electrically pumped all-graphene-contact micro-LED device at room temperature. A vertically *p*–*i*–*n* doped top-down-fabricated single

microdisk was on-demand align-transferred onto a device chip using PDMS-microtip-assisted transfer-printing. Top and bottom graphene contacts were lithographically patterned and introduced to the microdisk. EL spectroscopy revealed clear diode-like transport properties and typical *L–I* characteristics as well as an unpolarized angular distribution of EL. These results indicated considerable improvements in the device performance, as compared with that in our previous work. We believe that our all-graphene-contact approach can offer an efficient and robust current injection scheme for various on-demand transferred microstructures and help realize their instant electrification in PICs.

See the supplementary material for experimental details and supporting data, including the details of compositional materials, AFM topographic characterization, TLM experiment, temperature-dependent transport properties, and additional EL emission profiles.

Y.-S.N. acknowledges the support of this work by Konkuk University, 2018.

AUTHOR DECLARATIONS

Conflict of Interest

The authors have no conflicts to disclose.

Author contributions

Byung-Ju Min, Yeon-Ji Kim, and Jae-Hyuck Choi have contributed equally to this work.

Byung-Ju Min: Conceptualization (equal); Data curation (lead); Investigation (lead); Methodology (lead); Visualization (lead); Writing – Original draft (supporting); Writing – review and editing (equal). **Yeon-Ji Kim:** Data Curation (equal); Formal Analysis (equal); Methodology (equal); Software (lead); Writing – review and editing (equal). **Jae-Hyuck Choi:** Formal Analysis (lead); Project Administration (equal); software (equal); Writing – Original draft (lead); Writing – review and editing (equal). **Min-Woo Kim:** Visualization (supporting). **Kyong-Tae Park:** Formal Analysis (supporting); Software (supporting). **Dong Jin Jang:** Resources (supporting). **Jin Sik Choi:** Resources (supporting). **You-Shin No:** Conceptualization (lead); Funding Acquisition (lead); Project Administration (lead); Supervision (lead); Writing – Original draft (equal); Writing – review and editing (lead).

DATA AVAILABILITY

The data that support the findings of this study are available from the corresponding author upon reasonable request.

REFERENCES

[1]M. E. Stewart, C. R. Anderton, L. B. Thompson, J. Maria, S. K. Gray, J. A. Rogers, and R. G. Nuzzo, Chem. Rev. **108**, 494 (2008).
[2]W. Chen, Ş. K. Özdemir, G. Zhao, J. Wiersig, and L. Yang, Nature **548**, 192 (2017).
[3]Y.-S. No, Appl. Sci. **9**, 802 (2019).
[4]J.-H. Choi, W. E. Hayenga, Y. G. N. Liu, M. Parto, B. Bahari, D. N. Christodoulides, and M. Khajavikhan, Nat. Commun. **12**, 3434 (2021).
[5]E. L. Wooten, K. M. Kissa, A. Yi-Yan, E. J. Murphy, D. A. Lafaw, P. F. Hallemeier, D. Maack, D. V. Attanasio, D. J. Fritz, G. J. McBrien, and D. E. Bossi, IEEE J. Select. Top. Quantum Electron. **6**, 69 (2000).
[6]H. Ma, A. K.-Y. Jen, and L. R. Dalton, Adv. Mater. **14**, 1339 (2002).
[7]J. Zhang, G. Muliuk, J. Juvert, S. Kumari, J. Goyvaerts, B. Haq, C. Op de Beeck, B. Kuyken, G. Morthier, D. van Thourhout, R. Baets, G. Lepage, P. Verheyen, J. van Campenhout, A. Gocalinska, J. O'Callaghan, E. Pelucchi, K. Thomas, B. Corbett, A. Trindade, and G. Roelkens, APL Photonics **4**, 110803 (2019).
[8]A. Naiman, B. Desiatov, L. Stern, N. Mazurski, J. Shappir, and U. Levy, Opt. Lett. **40**, 1892 (2015).
[9]Q. Xu, B. Schmidt, S. Pradhan, and M. Lipson, Nature **435**, 325 (2005).
[10]R. Soref, IEEE J. Select. Top. Quantum Electron. **12**, 1678 (2006).
[11]G. Roelkens, L. Liu, D. Liang, R. Jones, A. Fang, B. Koch, and J. Bowers, Laser Photonics Rev. **4**, 751 (2010).
[12]K. J. Vahala, Nature **424**, 839 (2003).
[13]R.-M. Ma and R. F. Oulton, Nat. Nanotechnol. **14**, 12 (2019).
[14]Y. Kim, B. J. Park, M. Kim, D. I. Song, J. Lee, A. Yu, and M.-K. Kim, ACS Photonics **8**, 2590 (2021).
[15]D. Liang, M. Fiorentino, T. Okumura, H.-H. Chang, D. T. Spencer, Y.-H. Kuo, A. W. Fang, D. Dai, R. G. Beausoleil, and J. E. Bowers, Opt. Express **17**, 20355 (2009).
[16]F. Fan, Y. Yu, S. E. H. Amiri, D. Quandt, D. Bimberg, and C. Z. Ning, Appl. Phys. Lett. **110**, 171105 (2017).
[17]P. Rojo-Romeo, J. van Campenhout, P. Regreny, A. Kazmierczak, C. Seassal, X. Letartre, G. Hollinger, D. van Thourhout, R. Baets, J. M. Fedeli, and L. D. Cioccio, Opt. Express **14**, 3864 (2006).
[18]J. van Campenhout, P. Rojo-Romeo, P. Regreny, C. Seassal, D. van Thourhout, S. Verstuyft, L. D. Cioccio, J. M. Fedeli, C. Lagahe, and R. Baets, Opt. Express **15**, 6744 (2007).
[19]Y.-H. Kim, S.-H. Kwon, J. M. Lee, M.-S. Hwang, J.-H. Kang, W. I. Park, and H.-G. Park, Nat. Commun. **3**, 1123 (2012).
[20]S.-W. Park, M.-W. Kim, K.-T. Park, J.-H. Ku, and Y.-S. No, ACS Photonics **7**, 3313 (2020).
[21]D. Jevtics, J. A. Smith, J. McPhillimy, B. Guilhabert, P. Hill, C. Klitis, A. Hurtado, M. Sorel, H. H. Tan, C. Jagadish, M. D. Dawson, and M. J. Strain, Opt. Mater. Express **11**, 3567 (2021).
[22]H.-G. Park, C. J. Barrelet, Y. N. Wu, B. Z. Tian, F. Qian, and C. M. Lieber, Nat. Photonics **2**, 622 (2008).
[23]P. Fan, C. Colombo, K. C. Y. Huang, P. Krogstrup, J. Nygård, A. Fontcuberta i Morral, and M. L. Brongersma, Nano Lett. **12**, 4943 (2012).
[24]Y.-S. No, J.-H. Choi, H.-S. Ee, M.-S. Hwang, K.-Y. Jeong, E.-K. Lee, M.-K. Seo, S.-H. Kwon, and H.-G. Park, Nano Lett. **13**, 772 (2013).
[25]M. Tchernycheva, P. Lavenus, H. Zhang, A. V. Babichev, G. Jacopin, M. Shahmohammadi, F. H. Julien, R. Ciechonski, G. Vescovi, and O. Kryliouk, Nano Lett. **14**, 2456 (2014).
[26]M.-W. Kim, S.-W. Park, K.-T. Park, B.-J. Min, J.-H. Ku, J.-Y. Ko, J. S. Choi, and Y.-S. No, Nano Lett. **22**, 1316 (2022).
[27]B. Guilhabert, A. Hurtado, D. Jevtics, Q. Gao, H. H. Tan, C. Jagadish, and M. D. Dawson, ACS Nano **10**, 3951 (2016).
[28]V. Dolores-Calzadilla, B. Romeira, F. Pagliano, S. Birindelli, A. HigueraRodriguez, P. J. van Veldhoven, M. K. Smit, A. Fiore, and D. Heiss, Nat. Commun. **8**, 14323 (2017).
[29]Y. Akahane, T. Asano, B.-S. Song, and S. Noda, Nature **425**, 944 (2003).
[30]H. G. Park, S. H. Kim, S. H. Kwon, Y. G. Ju, J. K. Yang, J. H. Baek, S. B. Kim, and Y. H. Lee, Science **305**, 1444 (2004).
[31]L. Chang, Y. Li, N. Volet, L. Wang, J. Peters, and J. E. Bowers, Optica **3**, 531 (2016).
[32]M. A. Meitl, Z. T. Zhu, V. Kumar, K. J. Lee, X. Feng, Y. Y. Huang, I. Adesida, R. G. Nuzzo, and J. A. Rogers, Nat. Mater. **5**, 33 (2006).
[33]F. Bonaccorso, Z. Sun, T. Hasan, and A. C. Ferrari, Nat. Photonics **4**, 611 (2010).
[34]H. J. Park, J. Meyer, S. Roth, and V. Skákalová, Carbon **48**, 1088 (2010).
[35]A. Yadav, I. E. Titkov, G. S. Sokolovskii, S. Y. Karpov, V. V. Dudelev, K. K. Soboleva, M. Strassburg, I. Pietzonka, H. J. Lugauer, and E. U. Rafailov, J. Appl. Phys. **124**, 013103 (2018).